Bearing capacity of shallow footing under combined loading

Osamu Kusakabe[1]

Tomohide Takeyama[2]

[1] Professor, Dept. of Civil and Environmental Engineering, Tokyo Institute of Technology
[2] Assistant Professor, Dept. of Civil and Environmental Engineering, Tokyo Institute of Technology

SYNOPSIS: The paper deals with two bearing capacity problems of shallow footing under combined loading.   The first is a FEM study of shallow strip footing on two-layer clay deposits subjected to a vertical, horizontal and moment combined loading, while the second is a centrifuge study of shallow rectangular footing on dry sand under double eccentricity. The FEM results revealed that the existence of top soft layer sensitively affects more on horizontal and moment capacity than vertical capacity for cases of footing on soft clay overlying stiff clay. Practical design charts are presented to evaluate bearing capacities of footing for various combinations of the ratio of the depth of the upper layer to the footing width and the ratio of undrained strength of the upper layer to that of the lower. The centrifuge tests indicated that current design practice of calculating failure load of rectangular surface footing under double eccentricity underestimates the centrifuge loading test data. This trend is more marked when the eccentricity becomes larger. The decreasing trend in failure load with an increase of double eccentricity is rather uniquely expressed by a single curve, using a newly defined resultant eccentricity and the diagonal length of the footing base.

Keywords: Bearing capacity, Shallow footing, FEM analysis, Centrifuge test

1. Introduction

Over the last two decades, the issue of bearing capacity of shallow footing has been studied with respect to combined loading framework both from the viewpoints of physical and numerical modeling based on macro-element concept (e.g. Tan, 1990, Nova and Montransio, 1991, Butterfield and Gottardi, 1994). This paper deals with two bearing capacity problems of shallow footing under combined loading.

The first problem is a FEM study of bearing capacity of shallow strip footing on two layered clays under combined loading. The problem has a long history of research, starting from a classical solution for vertical bearing capacity of strip footing by limit equilibrium analysis, using circular slip surface by Button (1953). He adopted two parameters to describe the problem; the ratio of undrained shear strength in the bottom clay layer (c_b) to that of the top layer (c_t), and the ratio of depth measured from the base of footing to the interface of the two layers (D) to a half of footing width (B/2) and provided design charts in terms of bearing capacity factor, N_c, for two cases: (a) stiff clay overlying soft clay and (b) soft clay overlying stiff clay. Reddy and Srinivasan (1967) extended this analysis to anisotropic clays with a linear variation of shear strength with depth. Brown and Meyerhof (1969) criticized the use of circular slip surface based on a number of laboratory loading tests using strip and circular footings on various combinations of two layered clays, and provided charts for modified bearing capacity factors in terms of undrained shear strength ratio, c_b/c_t, and depth of top layer/footing width ratio, D/B. Chen (1975) also analyzed the Button's problem from the context of limit analysis using a rotational mechanism. Nakase et al.(1987) conducted a series of centrifuge tests on normally consolidated clay layer with a surface crust layer with upper bound analyses. Merifield et al.(1999) applied numerical limit analysis to evaluate the undrained bearing capacity of a rigid surface strip footing resting on a two-layer clay

deposit. Michalowski (2002) presented upper bound solutions to limit loads on strip footing over two-layer clay foundation soil, considering two failure mechanisms: one with a continually deforming field and the other with a multi-block mechanism. He then found that the multi-block mechanism yields the least upper bound. The method was also used for calculations of bearing capacity of strip footings subjected to loads with horizontal components. Wang and Carter (2002) conducted large deformation 2D FE analyses with the Arbitrary Lagrangian-Eulerain method on deep penetration behaviour of strip and circular footings overlying two different undrained clay layers, where the upper layer was always stronger than the lower layer. They reported that the movement of soil from beneath the footing significantly affects the bearing response. Zhu & Michalowski (2005) performed three dimensional finite element analyses for bearing capacity of rectangular footings on two-layer clay. More recently Kim et al. (2008) reported 1 g model test, looking into the problem of bearing capacity evaluation in the early stage of ground improvement in marine clay dredged deposits. They concluded that Brown & Meyerhof equation underestimated and Button equation overestimated the experimental results.

It has been known that there is a surface in load space that defines a failure envelop for the footing, which can be written in the form of $f(V/s_uA, H/s_uA, M/s_uAB)=0$, where V, H and M are vertical load, horizontal load and moment, respectively, and A the plan area of the footing, B the width of the footing and s_u the undrained shear strength of the soil beneath the base of the footing. The common sign conventions for loads and moments used are based on the right-handed axes and clockwise positive conventions, as is shown in Figure 1.
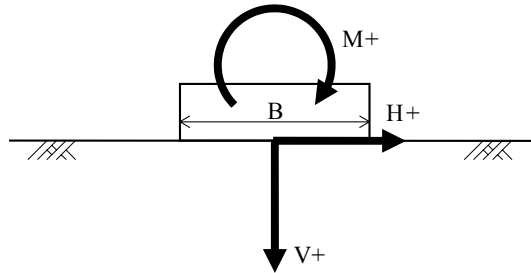
Figure 1. The common sign conventions for loads and moments

Bransby and Randolph (1998) conducted two dimensional finite element analyses, assuming that the clay obeys an elastic-plastic Tresca material with undrained shear strength linearly increasing with depth. The footing was assumed to adhere fully to the soil, which enables to develop compressive, tensile and shear stresses at the interface between the footing and the soil. Based on soil displacement fields by FEM, they developed upper bound mechanisms; wedge, scoop and combinations of them. They found that the shape of the failure envelop was found to be similar to that predicted by previous workers in V-M and V-H space but differed significantly in M-H space. That is, the failure envelop in M-H space is not symmetric, depending on the sign conventions of M and H. The combination of positive moment and negative horizontal load develops a simple scoop failure, whereas the combination of positive moment and positive horizontal load generates the wedge-scoop-wedge mechanism, resulting in the soil outside the footing base being pulled up sideways due to the adhesion between the footing base and the soil, associated with further mobilization of shear strength of the soil outside the footing base. Taiebat and Carter (2000) carried out three-dimensional finite-element analyses of circular footing on the surface of homogeneous, purely cohesive soil, under the similar assumption as those of Bransby and Randolph (1998). A three-dimensional failure locus was presented, and an equation that approximates the shape of the failure locus was also suggested as

$$F = \left(\frac{V}{V_u}\right) + \left[\frac{M}{M_u}\left(1-\alpha\frac{HM}{H_u|M|}\right)\right]^2 + \left|\left(\frac{H}{H_u}\right)^3\right| - 1 = 0 \qquad (1)$$

where α is a factor that depends on the soil profile, and V_u, M_u and H_u represents the capacity of the footing under pure vertical load, pure moment and pure horizontal load, respectively. They concluded that overall the approximation is

satisfactory, and the equation gives conservative and sufficient results for many practical applications. These studies are related to either a single clay layer of uniform strength or normally consolidated.

The second problem is a centrifuge study of shallow rectangular footing on dry sand under double eccentricity. A typical combined loading situation encountered in practical design is eccentric loading. The concept of effective width for a strip footing proposed by Meyerhof (1953) has been commonly used in the analysis of foundations subjected to eccentric loading (Poulos et al., 2001). The concept of effective width can be stated that the bearing capacity of a strip footing with a width of B subjected to an eccentrically applied vertical loading with the eccentricity of e is assumed to be equivalent to the bearing capacity of another strip footing with a fictitious effective width B' (where B' = B - 2e) on which the vertical load is centrally applied. For the case of strip footing on sand, this effective width concept can be expressed in terms of failure envelope in vertical load (V) - moment (M) space as $M/B = 0.5V\{1 - (V/V_u)^{0.5}\}$, where V_u is the failure vertical load under pure vertical loading, and V the vertical failure load with eccentricity.

Meyerhof (1953) extended the effective width concept to the effective area concept for a rectangular footing of length L and width B with double eccentricity, e_L and e_B on the major axes by finding the minimum effective contact area with a straight boundary across the footing base such that its centroid coincides with that of the load. The effective contact areas are, thus, assumed either a trapezoidal or triangular shape under double eccentricity.

Some current design specifications (e.g. Japan Road Association, 2002) conveniently modify the original Meyerhof's effective area in such a way that the contact area remains a rectangular shape with the effective length L' (= L - 2e_L) and the effective width B' (= B - 2e_B), as shown in Figure 2. The effective width concept has been well supported by various experimental results, mainly for single eccentricity, both under gravitational and centrifugal acceleration fields as a conservative hypothesis (e.g. Terashi et al., 1984; Okamura et al., 2002; Musso and Ferlisi, 2009). Thus it seems that there exist no practical questions regarding the evaluation of ultimate bearing capacity as far as strip footing with single eccentricity is concerned. It has been reported, however, that two types of failure mode have been observed: failure occurs either (A): on the side of the eccentricity of the load or (B): on the opposite side of the eccentricity of the load as is illustrated in Figure 3.
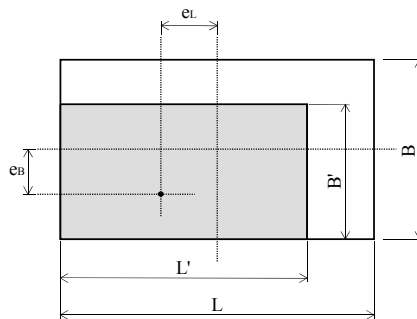
Figure 2. Illustration of effective area concept with length L'(=L-2e_L) and width B'(=B-2e_B)

Type A failure mode
(Meyerhof, 1953; Eastwood, 1955;
Purkayastha and Char, 1977)

Type B failure mode
(Jumikis, 1956; Kitazume, 1984)
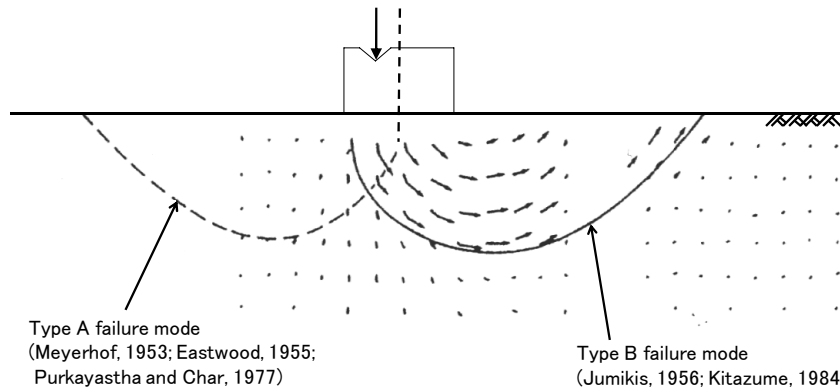
Figure 3. Two types of failure mode (Kitazume, 1984)

Kitazume (1984) suggested that the restriction of horizontal footing movement may be a possible reason for the occurrence of the two types of failure mode by conducting centrifuge tests and FEM analyses. Kitazume and Ikeda (1993) performed two further types of loading tests in a centrifuge, one with a horizontal restriction and the other without restriction by monitoring the horizontal force generated at the footing base during loading. They observed that the footing tends to horizontally displace towards the side of eccentricity as well as vertically settle when the horizontal force is kept zero. When the horizontal movement is restricted, the horizontal force towards the center of the footing is generated at the base of footing to compensate the restriction and the ultimate bearing capacity reduction is about 10 % larger than that of without restriction. Hence the failure mode was considerably affected by the horizontal restriction. When the horizontal movement is restricted, the failure surface predominantly occurs on the opposite side of the eccentricity. When the footing is free to move horizontally, the failure surface develops towards the side of the eccentricity with a smaller failure surface on the opposite side.

Compared with a number of experimental studies, studies of theoretical verification for the effective width concept are limited. As far as the authors are aware of, only work by Narita and Yamaguchi (1988) analytically derived Meyerhof's concept of effective width for strip footing, assuming that the failure surface is expressed by a single logarithmic spiral.

The literature review reveals that very limited information regarding double eccentricity is available, which is essentially three dimensional in nature.

2. FEM study of shallow strip footing on two-layer clay under combined loading

Figure 4 shows a typical finite-element mesh in the plane strain condition. The ground was assumed to be a level ground with two horizontally layered cohesive deposits. The footing width (B) was taken to be 160mm, and the area of analysis was about 9B in width and 2.5B in depth, to minimize possible boundary effects. At the boundaries, the vertical and horizontal displacements at the bottom boundary were fixed, as were the horizontal displacements at the side boundaries. The footing base was assumed to be adhering fully to the soil.
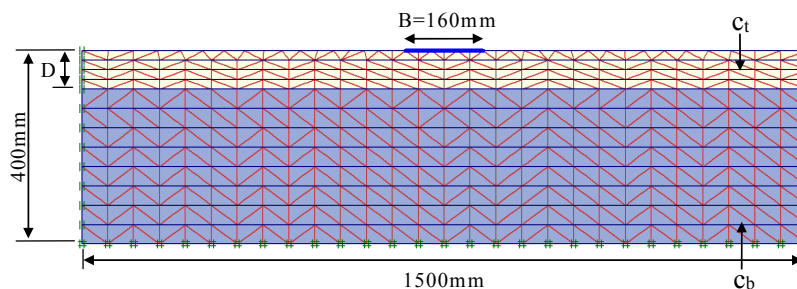
Figure 4. Typical FE mesh used

The element used was a 15-node triangle. The element stiffness matrix was evaluated by numerical integration using a total of 12 Gauss points. There were 684 elements, 5657 nodes and 8208 Gauss points in the mesh shown in Figure 4. The program used was a commercially available two-dimensional FEM program, Plaxis version 8(reference).

Since undrained bearing failure was considered in this study, the soil was assumed to be an elastic perfectly plastic material, obeying Tresca failure criterion. Two groups of layered ground were studied: (a) stiff clay overlying soft clay and (b) soft clay overlying stiff clay. The undrained shear strength of stiff clay was assumed to be a fixed value of 80 kN/m^2 and the undrained shear strength of soft clay varied from 20 to 60 kN/m^2, covering the values of c_b/c_t ratio from 0.25 to 0.75 for the cases of stiff clay overlying soft clay, and from 1.33 to 4.0 for the cases of soft clay overlying stiff clay. The effect of two layered ground is expressed by the D/B ratio. The value of D/B varies from 0 to 2.0. In total, 30 cases were calculated. The values of other geotechnical parameters used for the FEM analysis are listed in Table 1.

Table 1. Input parameters

Unit weight	Young's modulus	Undrained shear strength		Poisson's ratio
		for stiff clay	for soft clay	
γ(kN/m^3)	E(kN/m^2)	(kN/m^2)	(kN/m^2)	ν
16	50,000	80	20, 40, 60	0.495

2.1 Key results and discussion

2.1.1 Bearing capacity of footing on stiff clay overlying soft clay: $c_b/c_t < 1$

Figure 5 plots the value of H/s_uA against V/s_uA at failure for various values of D/B in the range from 0 to 2 for the case of c_b/c_t=0.25, where s_u is equal to the undrained shear strength of the top clay layer, c_t, and A is the bottom plan of the footing (A=B*1). The case of D/B=0 corresponds to the single clay layer with the undrained shear strength of the bottom layer, c_b. V/s_uA can be regarded as bearing capacity factor, N_c. The value of V/s_uA at the horizontal axis (under pure vertical loading) is 5.35 for D/B=2.0 and 1.34 for D/B=0, four times difference between the two, as was expected from the condition of c_b/c_t=0.25. The value of H/s_uA at the vertical axis (under pure horizontal loading) is 1.1 for D/B=2.0 and 0.3 for D/B=0, once again four times difference. Hereafter the value of V at the horizontal axis and the value of H at the vertical axis are denoted as V_u and H_u, respectively for a given D/B value.
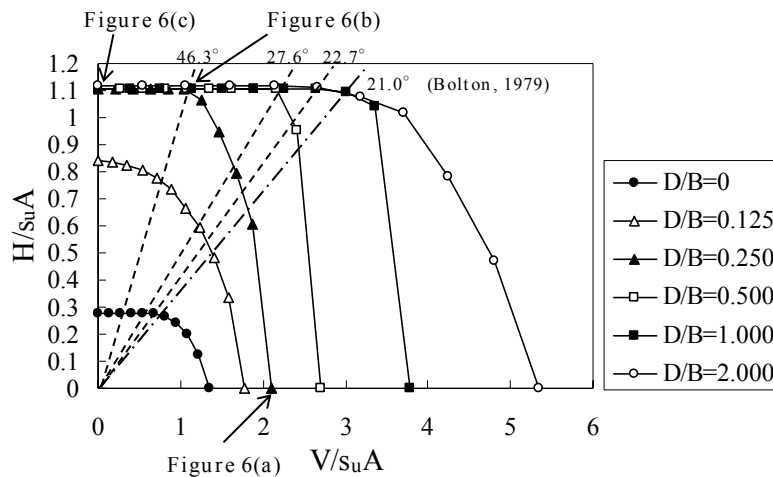
Figure 5. Failure Envelopes in H-V Space (c_b/c_t=0.25)

Although the bearing capacity factor N_c obtained is about 4% larger than the plastic solution of $(2 + \pi)$, it is considered that the present study provides the consistent results and normalized values of V/V_u and H/H_u gives meaningful practical information.

Under the combined loading conditions, any horizontal load results in a drop of vertical resistance with an abrupt drop in vertical resistance, when the angle of loading inclination, defined by $\tan^{-1}$(H/V) becomes around 20° for the case of D/B=0 and 2.0. This result is very much consistent with the value of 21° for a single clay layer theoretically derived by Bolton (1979). Vertical bearing capacity (V_u) is sensitively influenced by existence of the bottom soft clay layer, resulting in significant decrease when D/B decreases. In contrast, the horizontal bearing capacity (H_u) remains unaffected until D/B value becomes smaller than 0.25. It is seen that the values for D/B=1.0, 0.5 and 0.25 are identical to those of D/B=2.0 until the angle of loading inclination becomes around 22.7°, 27.6°, 46.3°, respectively.

The change of bearing capacity is always associated with the change in failure mode. Figure 6 shows three displacement fields with different angles of loading inclination. As the angel of loading inclination increases, the failure mode changes from classical indentation mode to the wedge mode and finally to the slip mode where the slip surface is formed just beneath the footing.

(a) Pure vertical loading (scale factor = 5)

(b) Loading inclination: tan-1(V/H) = 46.3° (scale factor = 20)

(c) Pure horizontal loading (scale factor = 20)
Figure 6. Failure mode (D/B=0.25, c_b/c_t=0.25)
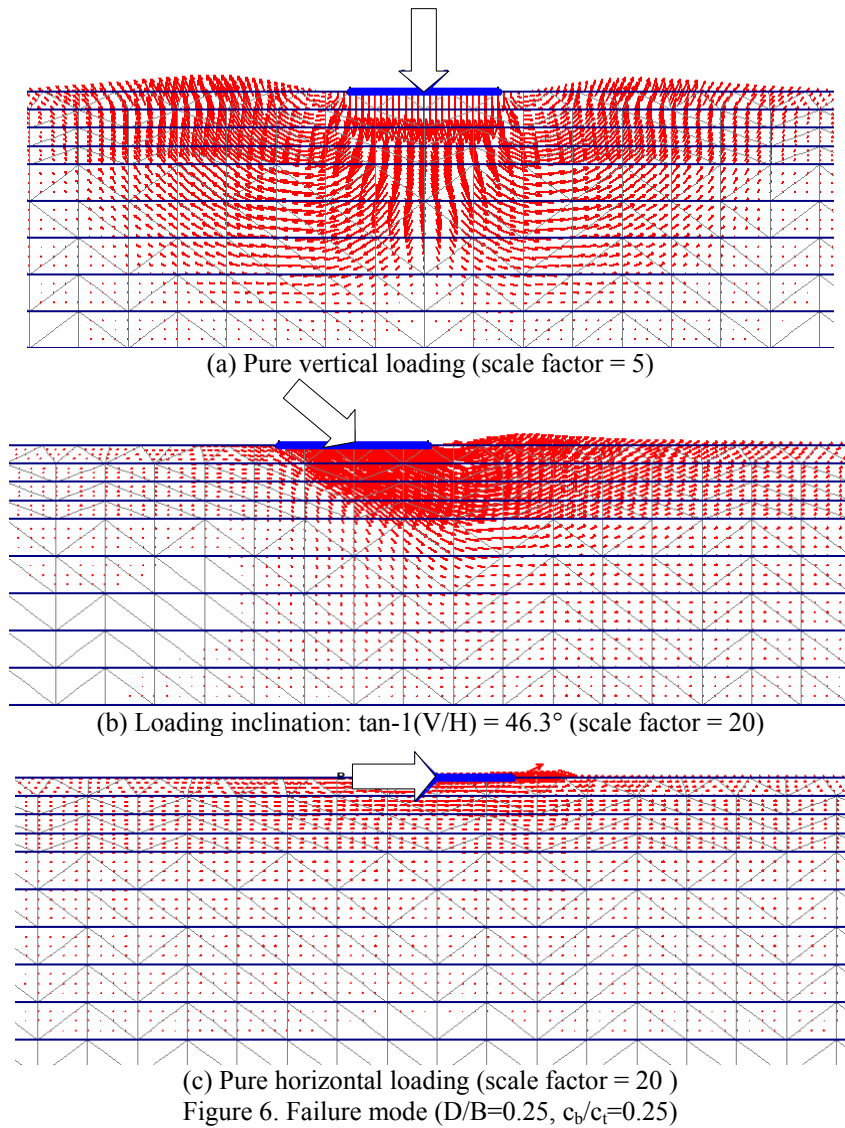
The normalized form of failure envelop, H/H_u-V/V_u space, is presented in Figure 7. The normalized failure envelops for D/B=2.0 and 0 are identical, both of which corresponds to the problems of the single clay layer. As D/B increases from D/B=0, the failure envelop first shrinks and then starts expanding until D/B becomes 1.0, and it shrinks again towards that of single clay layer.

Figure 7. Normalized failure envelopes in H-V space (c_b/c_t=0.25)
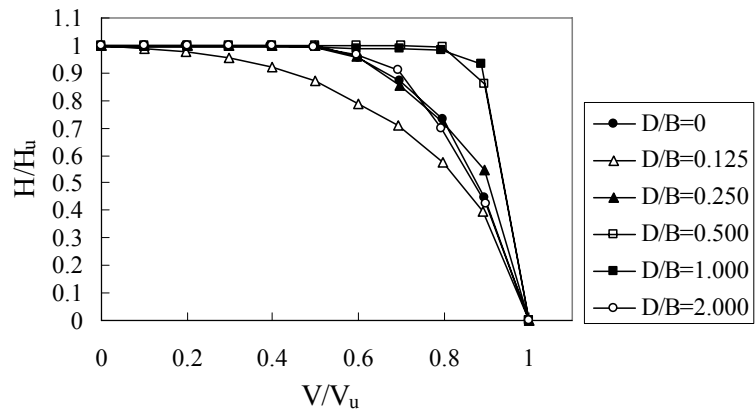
Figure 8 plots the value of M/s_uAB against V/s_uA at failure for various values of D/B in the range from 0 to 2 for the case of $c_b/c_t=0.25$. The value of M/s_uAB is 0.8 for D/B=2.0 and 0.2 for D/B=0, once again four times difference. Under the V-M combined loading conditions, any moment load results in a gradual drop of vertical resistance. It is noted that the values for D/B=1.0 are identical to those of D/B=2.0 until the angle defined by $\tan^{-1}(M/B/V)$ becomes around 16.6°.
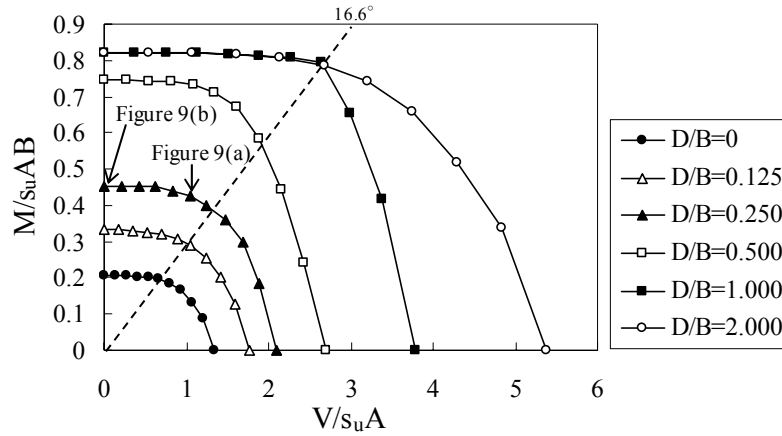
Figure 8. Failure envelopes in M-V space ($c_b/c_t=0.25$)

Figure 9 compares the displacement fields between a combined loading with positive vertical and positive moment (a) and the pure positive moment loading (b). The displacement fields suggest that critical failure mode changes from the wedge mode to the scoop rotational mode. The depth of rotational surface extends to 80% of the footing width.

(a) Positive vertical and positive moment loading
(scale factor = 2)

(b) Pure positive moment loading
(scale factor = 1)
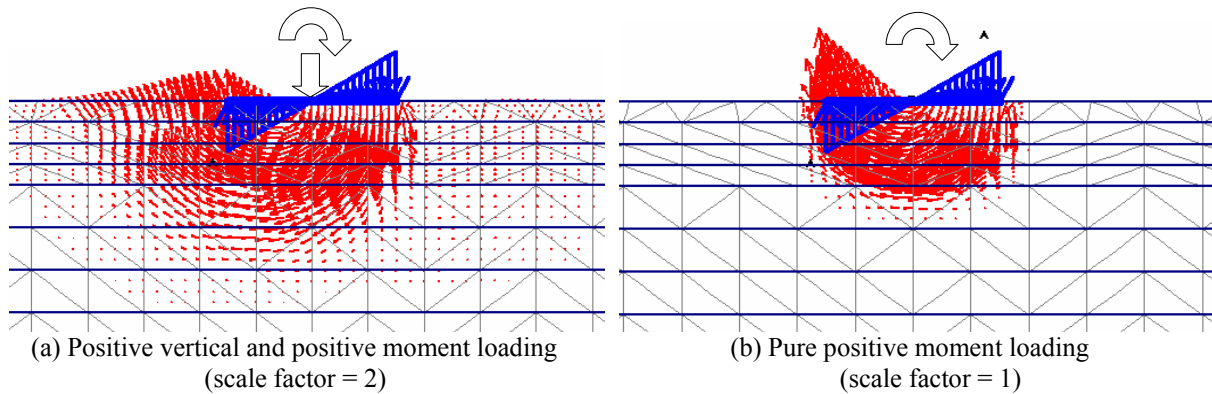
Figure 9. Failure mode (D/B=0.25, $c_b/c_t=0.25$)

Figure 10 plots the value of M/s_uAB against H/s_uA for various values of D/B in the range from 0 to 2 for the case of $c_b/c_t=0.25$. It is noted that moment capacity slightly increases with application of horizontal load for the case of single layer (D/B=2.0 and 0), whereas moment capacity slightly decreases with application of horizontal load for other cases. As will be seen later, however, the decrease in moment capacity with increasing horizontal load is observed only for the cases of c_b/c_t value being small.
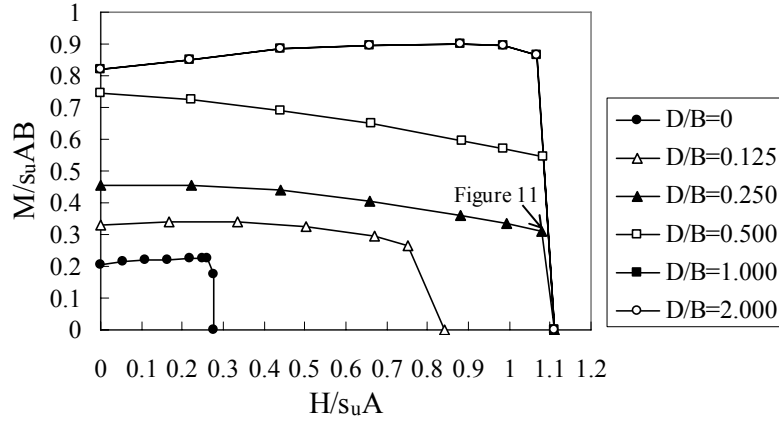
Figure 10. Failure envelopes in M-H space (c_b/c_t= 0.25)

Figure 11 shows the displacement field for the case of positive moment and positive horizontal loading. The failure mode seems to belong to the scoop rotational mode. The depth of rotational surface extends to a depth of 100% of the footing width which may be compared with 80% in Figure 9(b).
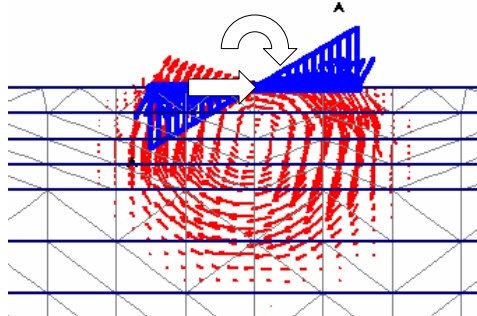
Figure 11. Failure mode (D/B=0.25, c_b/c_t=0.25, scale factor = 0.5)

In order to examine the effect of c_b/c_t value, Figure 12 shows the cases of c_b/c_t= 0.75. It is apparent by comparing with Figures 5, 8 and 10 that the smaller value of c_b/c_t significantly influences on the shape of failure surface than the larger value of c_b/c_t does. The effect of c_b/c_t is more marked in M-H plane.

(a) H-V space

10
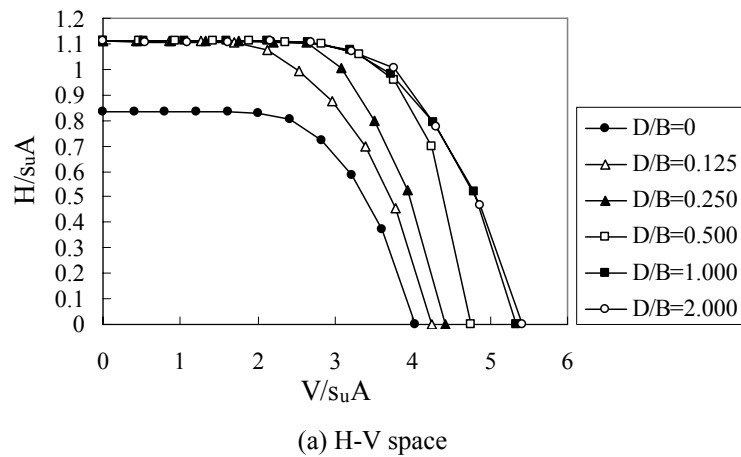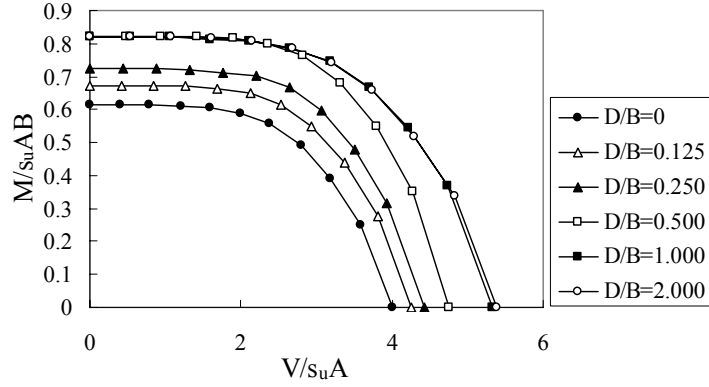
(b) M-V space
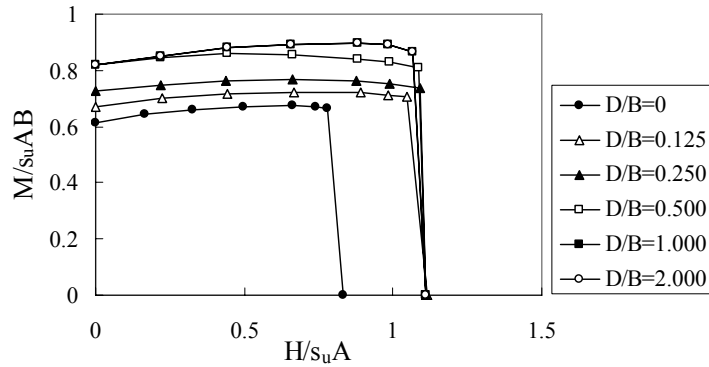
(c) M-H space

Figure 12. Failure envelopes (c_b/c_t=0.75)

2.1.2 Bearing capacity of footing on soft clay overlying stiff clay $c_b/c_t>1$

Figure 13 plots the value of H/s_uA against V/s_uA for various values of D/B in the range from 0 to 2 for the case of c_b/c_t=2.0. For the case of D/B=0 (uniform undrained shear strength of c_b), the vertical bearing capacity (V_u) gradually decreases with increasing D/B value. But the horizontal bearing capacity (H_u) suddenly drops to a half when D/B changes even from 0 to 0.125, indicating that the existence of thin soft layer drastically changes the horizontal bearing capacity. If a thin layer of soft clay exists on the top layer, the horizontal resistance (H_u) is governed by the value of c_t, whereas the vertical bearing capacity (V_u) is less sensitive to the existence of thin soft layer. The values for D/B from 0.125 to 2.0 are identical to those of D/B=2.0 until the angle of loading inclination, defined by $\tan^{-1}(H/V)$ becomes around 18.7°.
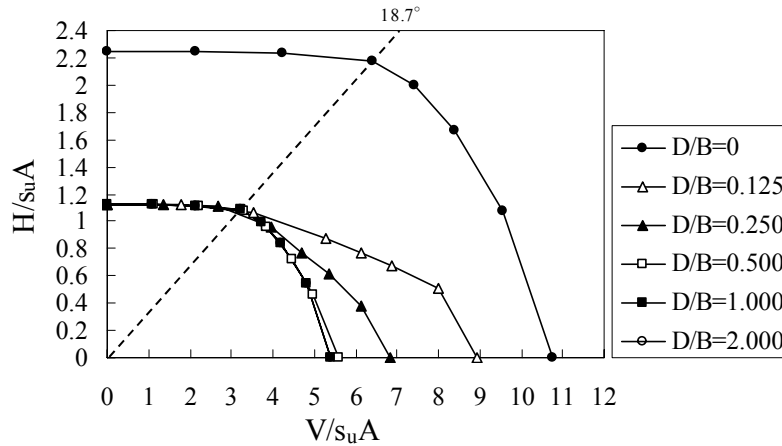
Figure 13. Failure envelopes in H-V space (c_b/c_t=2.0)

11

Normalized failure envelops for 0<D/B<2.0 are located within those of the single clay layer, as is seen in Figure 14.
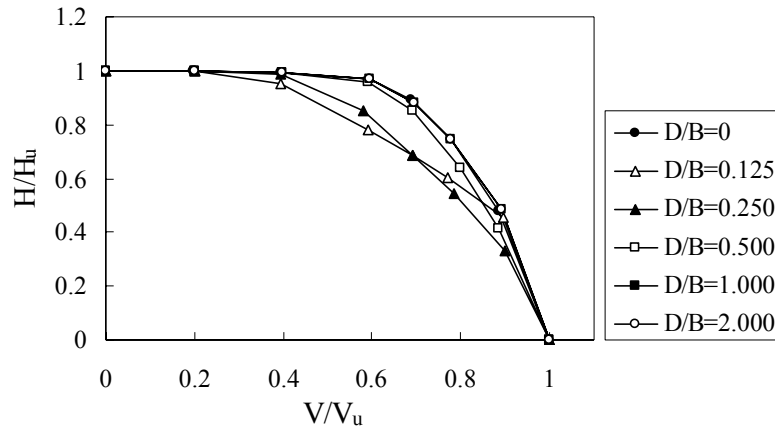
Figure 14. Normalized failure envelopes in M-H space (c_b/c_t=2.0)

Figure 15 plots the value of M/s_uAB against V/s_uA for various values of D/B in the range from 0 to 2 for the case of c_b/c_t=2.0. It can be seen that the failure surface gradually becomes smaller as D/B increases. Similar to V-H plane, normalized failure envelops for 0<D/B<2.0 are located within those of the single clay layer, as is seen in Figure 16. It should be noted here that there is a slight difference between the values of D/B=0.0 and 2.0. Figure 17 plots the value of M/s_uAB against H/s_uA for various values of D/B in the range from 0 to 2.0 for the case of c_b/c_t=2.0. In this series of analysis, the combined loading with positive moment and negative horizontal load was also considered. It is noted that the shape of interaction diagram of positive moment and positive horizontal loading significantly differ from that of positive moment and negative moment loading. Application of negative horizontal load results in gradually drops of moment capacity, whereas positive horizontal loads lead to slightly increase in moment capacity. This result is consistent with the results (Bransby and Randolph, 1998; Taiebat and Carter, 2000). Figure 18 presents the normalized failure envelops.
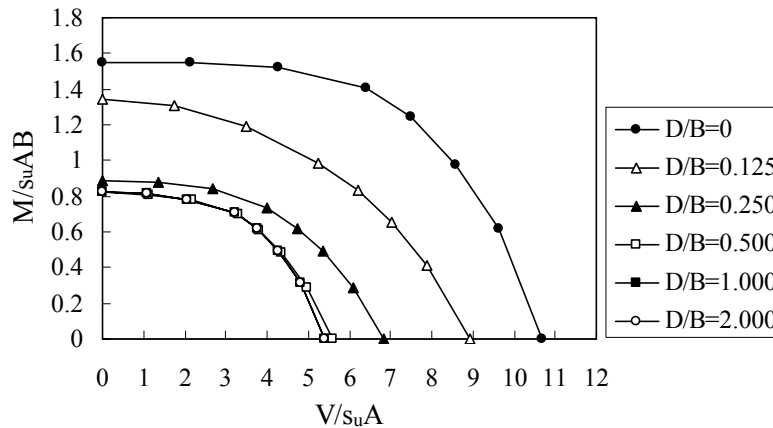
Figure 15. Failure envelopes in M-V space (c_b/c_t=2.0)
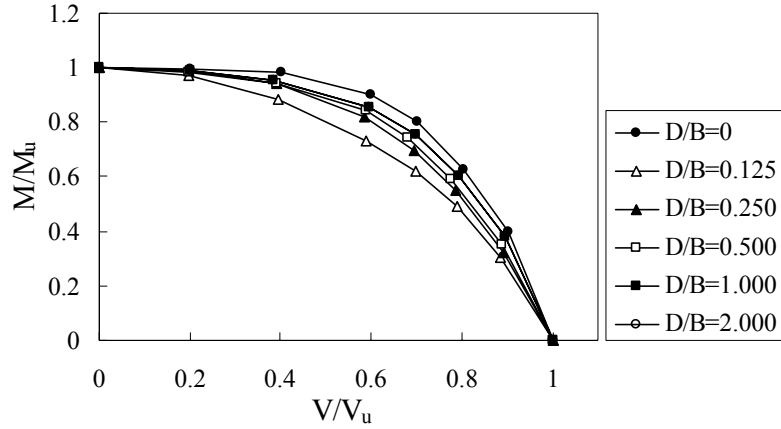
Figure 16. Normalized failure envelopes in M-V space ($c_b/c_t=2.0$)
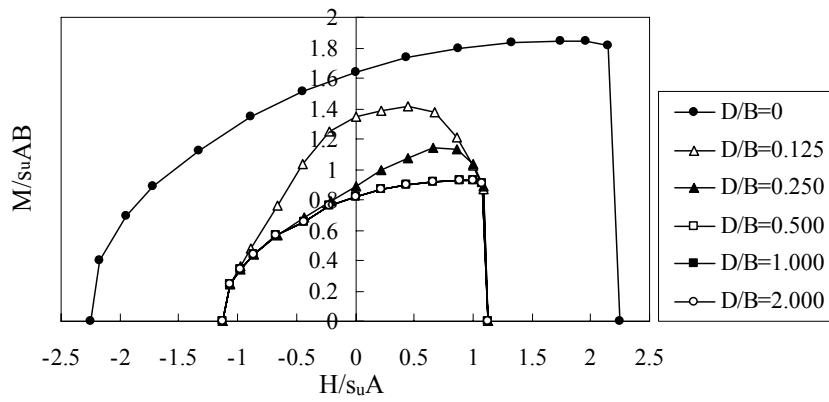
Figure 17. Failure surfaces in M-H space ($c_b/c_t=2.0$)
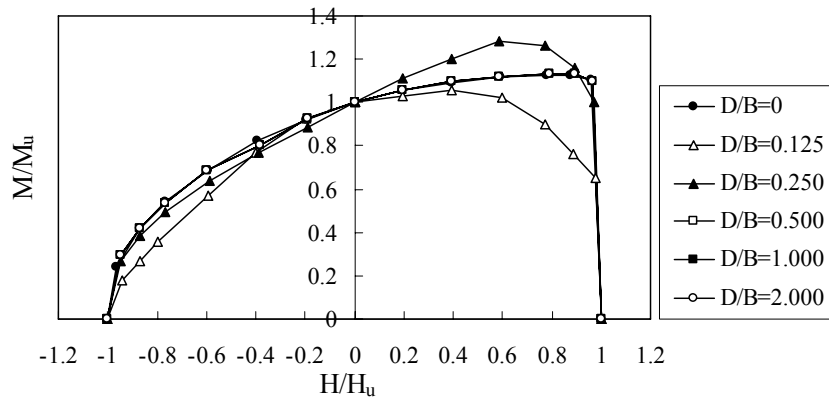
Figure 18. Normalized failure envelopes in M-H space ($c_b/c_t=2.0$)

2.2 Evaluation of bearing capacity

As have been discussed, the thin soft clay in the top layer sensitively influences on the shape of failure surface, which poses a difficulty in developing a simple yet practical proposal for an equation describing failure surface. An attempt was made, therefore, to develop equations only for the cases of footing on stiff clay overlying soft clay. Taiebat and Carter (2000) proposed the equation for failure surface of footing under combined loading and suggested to use α=0.3 in Equation (1), which gives a reasonable value for single layer. As have been previously discussed, the modification is required to accommodate the effect of c_b/c_t and D/B on the failure surface in M-H plane as $c_b/c_t<1$

13

$$\alpha = 0.25 - 1.45\frac{D}{B}\left(\frac{c_b}{c_t} - 0.84\right) \quad \text{when D/B<1.0 and } c_b/c_t<0.84, \text{ MH>0} \tag{2}$$

$$\alpha = 0.25 \qquad\qquad \text{when D/B>1.0 or } c_b/c_t>0.84, \text{ MH<0} \tag{3}$$

Figure 19 presents the chart for vertical bearing capacity factor. The equation for vertical bearing capacity proposed by Brown and Meyerhof (1969) is well supported by the present study, although the present study gives about 4% larger values. It is thus acceptable to adopt their bearing capacity formula for practical use.
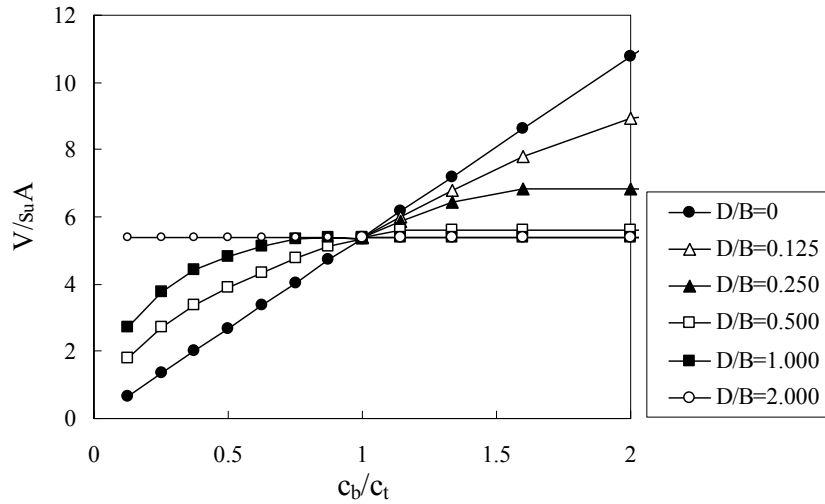
Figure 19. Chart for vertical capacity factor

$$\frac{V_u}{s_u A} = 5.34\left\{1-\left(1-\frac{c_b}{c_t}\right)\left(1-0.5\frac{D}{B}\right)\right\} \le 5.34 \quad \text{when } c_b/c_t<1 \tag{4}$$

$$\frac{V_u}{s_u A} = 5.34\left\{1+\left(\frac{c_b}{c_t}-1\right)\left(1-2.0\frac{D}{B}\right)\right\} \ge 5.34 \quad \text{when } c_b/c_t>1 \tag{5}$$

As was pointed out, the horizontal bearing capacity was highly sensitive to the strength of top clay layer. As is seen in Figure 20 as the chart of horizontal capacity, horizontal capacity is proportional to the strength ratio, c_b/c_t for the case of D/B=0.0 and is constant regardless of c_b/c_t for the cases of D/B more than 0.25. Only the situations where c_b/c_t being less than 0.75 and D/B = 0.125, need to consider nonlinearity. The following equation is proposed for practical use.

$$\frac{H_u}{s_u A} = \frac{c}{s_u A} \qquad \begin{cases} c = c_t & D/B > 0.25 \\ c = c_b & D/B < 0.25 \end{cases} \qquad \text{when } c_b/c_t<1 \tag{6}$$

$$\frac{H_u}{s_u A} = \frac{c_t}{s_u A} \qquad\qquad \text{when } c_b/c_t>1 \tag{7}$$

14
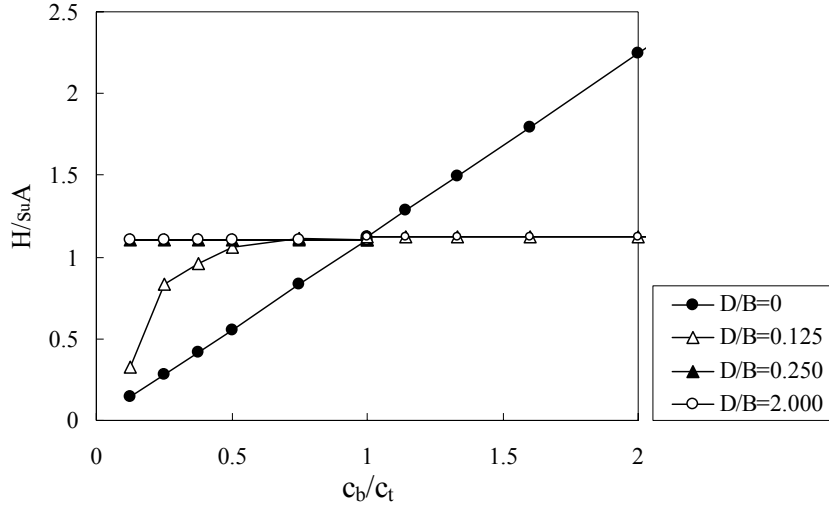
Figure 20. Chart for horizontal capacity factor

Figure 21 shows the chart for moment capacity factor. The following equation can fit the analytical results and is proposed to use for practical purpose.

$$\frac{M_u}{s_u AB} = 0.82\left\{1 - \left(1 - \frac{c_b}{c_t}\right)\left(1 - 1.33\frac{D}{B}\right)\right\} \le 0.82 \quad \text{when } c_b/c_t < 1 \tag{8}$$

$$\frac{M_u}{s_u AB} = 0.82\left\{1 + \left(\frac{c_b}{c_t} - 1\right)\left(1 - 3.5\frac{D}{B}\right)\right\} \ge 0.82 \quad \text{when } c_b/c_t > 1 \tag{9}$$
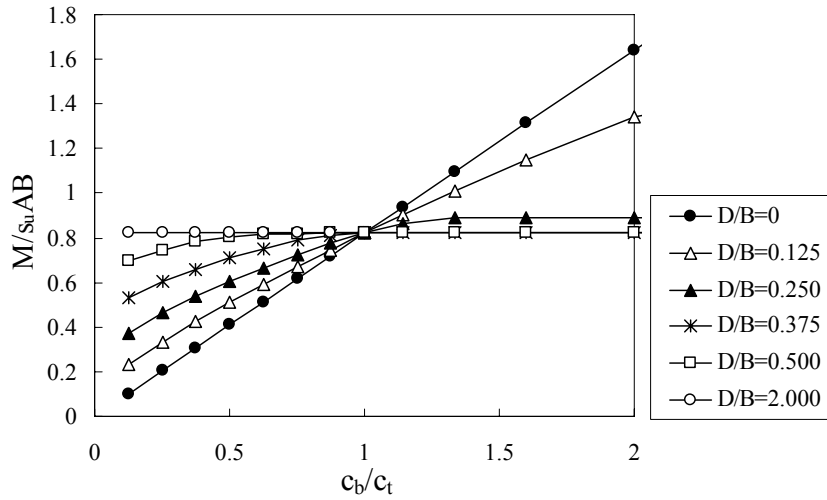
Figure 21. Chart for moment capacity factor

3. Centrifuge study of shallow rectangular footing on dry sand under double eccentricity

A series of centrifuge tests were conducted using the Mark III centrifuge of the Tokyo Institute of Technology. Model grounds were prepared in a circular steel container of dimensions 586 mm diameter and 400 mm deep. Air dry Toyoura

15

sand was used to make the model ground 200 mm deep with a target relative density of 80 % by air pluviation method. Table 1 summarizes the properties of Toyoura sand.

A 691 gram mass rectangular model footing was made of duralumin and has the dimensions of H 50 mm high, B 50 mm wide, and L 100 mm long, giving the aspect ratio (n = L/B) of 2. The footing thus is considered rigid. Sandpaper was glued to the base of the footing to simulate the rough footing base condition. A grid of 8 mm diameter semi-circular indents were made on the top surface of the footing with a spacing of 15 mm for the longer axis of footing and 10 mm for the shorter axis, which provide the contact points with a loading rod, of which the tip has a 7 mm diameter semi-circular shape to create the rotational free condition. Figure 22 shows the model footing with a numbering sequence for the loading points. The loading system used consists of a 5 ton capacity actuator driven by a 200 W motor and a supporting H beam frame which is firmly bolted on the web of the circular container. Therefore the loading point is restricted from horizontal displacement. Vertical load was measured by a load cell of 20 kN capacity attached to the loading rod. Vertical settlements of the footing were measured by a potentiometer attached to the loading rod. Horizontal displacements of the footing were measured by two laser displacement gauges at different elevations in the diagonal directions; front and side of the footing, from which the complete three dimensional movement of the footing can be captured. The vertical movement of the ground surface was also monitored by a number of potentiometers located around the footing.
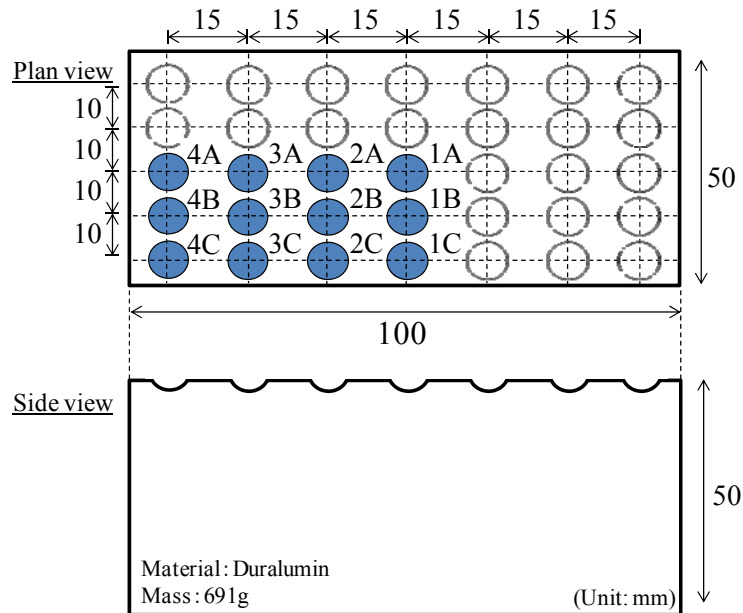
Figure 22. Model footing and loading point

The model footing was loaded under the centrifugal acceleration of 50 g. The loading rate of 5.0 mm/min was selected after comparing the load settlement curve of the loading rate of 0.5 mm/min and that of 5.0 mm/min, which follow almost an identical load settlement curve. Figure 23 illustrates the model ground with the loading system and measurement arrangements.
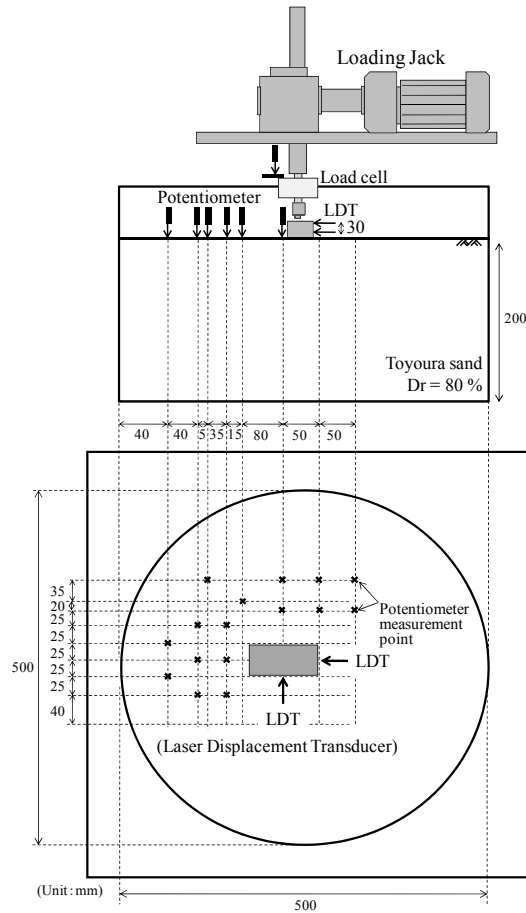
Figure 23. Model ground with the loading system and measurement arrangements

A particular emphasis was made to observe the detailed three dimensional failure surfaces after the loading test, by vertically dissecting the model ground at various sections to establish the failure surface. In order to do this, the top 100 mm of the model ground layer consisted of alternative layers of 5 mm thick colored Toyoura sand layer and 5 mm thick original Toyoura sand layer for the three cases 15, 16 and 17. After the loading test, some amount of water was introduced to the model ground under the gravitational acceleration through the bottom of the container up to the top surface of the ground and then the water was allowed to drain out of the container to generate an apparent cohesion in the model ground to keep the vertical cut face stable. A series of photographs were taken at each vertical section. Figure 24 presents the locations of the observed sections with views of typical dissected section. Together with the data of the vertical movement of the ground surface, three dimensional failure modes can be established. Table 2 summarizes the test program with test code, of which $\overline{e}$ will be defined later.

(a) for 4A (Case16)

(b) for 4C (Case17)
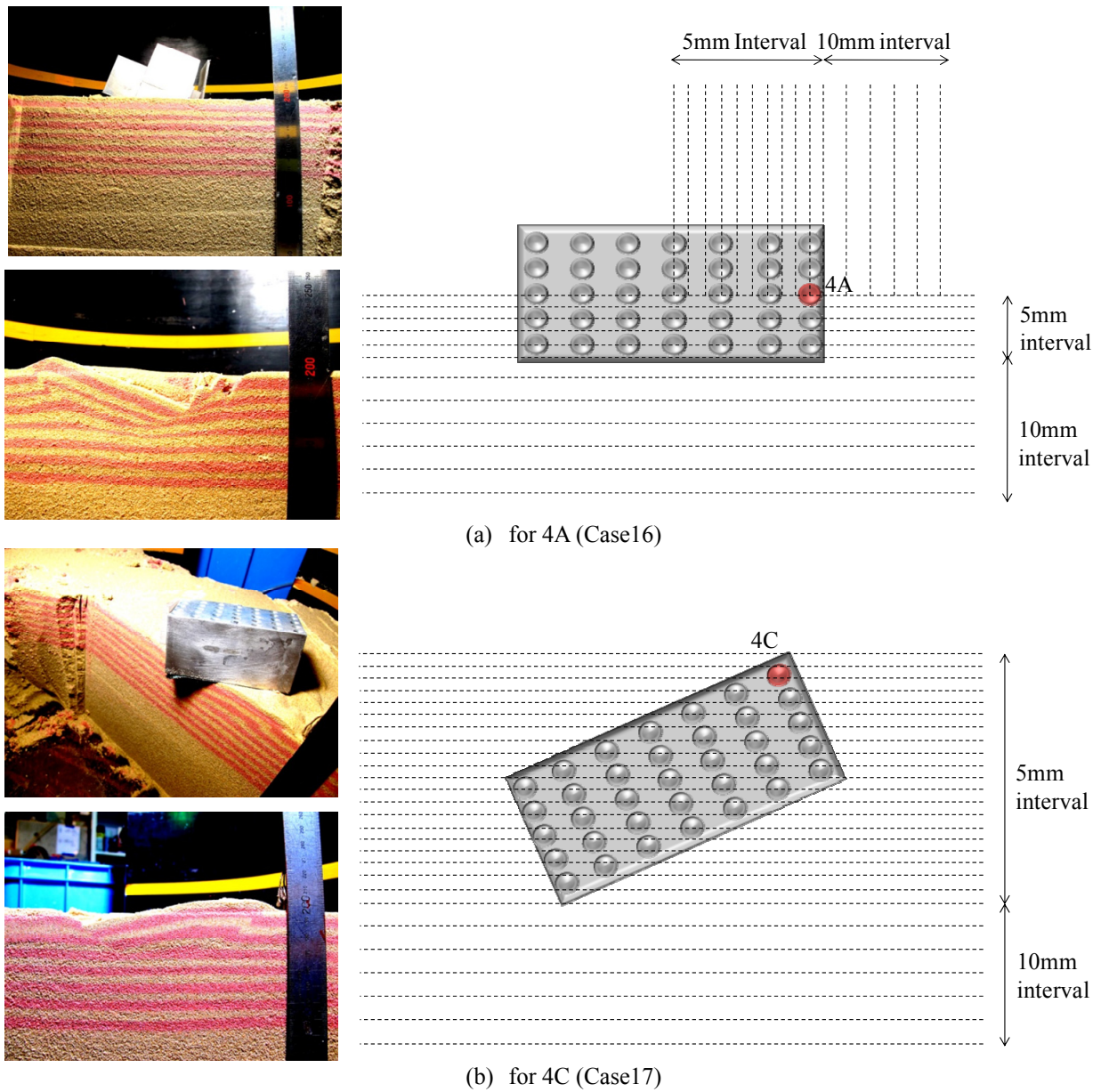
Figure 24. Locations of the observed sections with a view of typical dissected section

Table 2. Test program

Test code	Loading point	e_B (mm)	e_L (mm)	$\bar{e}$ (mm)	Dr (%)	Colored sand layer
Case 1	1A	0	0	0.0	80.4	NA
Case 2	1A	0	0	0.0	80.1	NA
Case 3	1B	10	0	22.4	79.4	NA
Case 4	1C	20	0	44.7	81.1	NA
Case 5	2A	0	15	16.8	78.9	NA
Case 6	2B	10	15	28.0	78.3	NA
Case 7	2C	20	15	48.1	78.3	NA
Case 8	3A	0	30	33.5	82.7	NA

Case 9	3B	10	30	40.2	81.4	NA
Case 10	3C	20	30	55.9	78.3	NA
Case 11	4A	0	45	50.3	79.2	NA
Case 12	4B	10	45	54.8	80.5	NA
Case 13	4C	20	45	67.1	81.3	NA
Case 14	4C	20	45	67.1	80.1	NA
Case 15	1C	20	0	44.7	76.1	○
Case 16	4A	0	45	50.3	80.5	○
Case 17	4C	20	45	67.1	82.5	○

3.1 Key Results and discussions

Figure 25 shows notations and conventions used in this paper: V is vertical load, M moment, δv vertical displacement, δh horizontal displacement and $\delta \theta$ angle of rotation measured from the vertical axis.
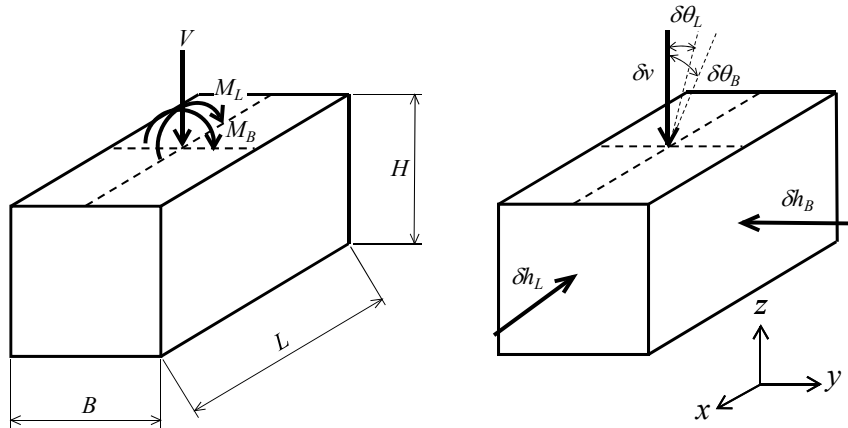
Figure 25. Notations and convections

In order to consider single and double eccentricity in a unified manner, a new index for eccentricity, termed resultant eccentricity hereafter, is defined as

$$\overline{e} = w\sqrt{\left(\frac{e_B}{B}\right)^2 + \left(\frac{e_L}{L}\right)^2} \ . \tag{10}$$

Also, the diagonal length of the rectangular footing base was used to normalize eccentricity.

$$w = \sqrt{B^2 + L^2} \tag{11}$$

Although there may be other alternative reference lengths for normalizing eccentricity, the diagonal length of the footing, w, was selected in this study based on the observations on the extent of the failure zone, as will be presented later.

Figure 26 shows two pairs of load-settlement curves for the cases of Case 1 and 2 (loading point A1, central loading) and Case 13 and14 (4C, eccentric loading) to confirm the repeatability of the test with satisfactory results.
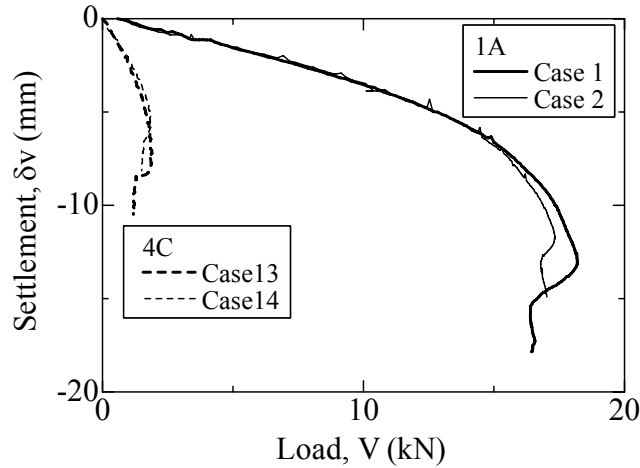
Figure 26. Confirmation of the repeatability for 1A (central loading) and 4C (eccentric loading)

Figure 27 shows the load-settlement curves for the cases of single eccentricity (Case 5 (2A), Case 8 (3A), Case 11 (4A), Case 3 (1B) and Case 4 (1C)) together with the case of central loading (Case 1 (1A)) for comparison. The settlements were normalized by either the footing width B or the footing length L, depending on the direction of the eccentricity. The observation that the failure load, the vertical stiffness and the settlement at failure decrease as the eccentricity increases is consistent with the previous centrifuge loading tests (Kitazume and Ikeda, 1993, Okamura et al., 2002). Terashi et al. (1984) gathered the previous model test data of the eccentric loading together with their own centrifuge test data and presented the whole data of the ratio of ultimate bearing capacity under eccentricity (q_e) and that of without eccentricity (q) against e/B.
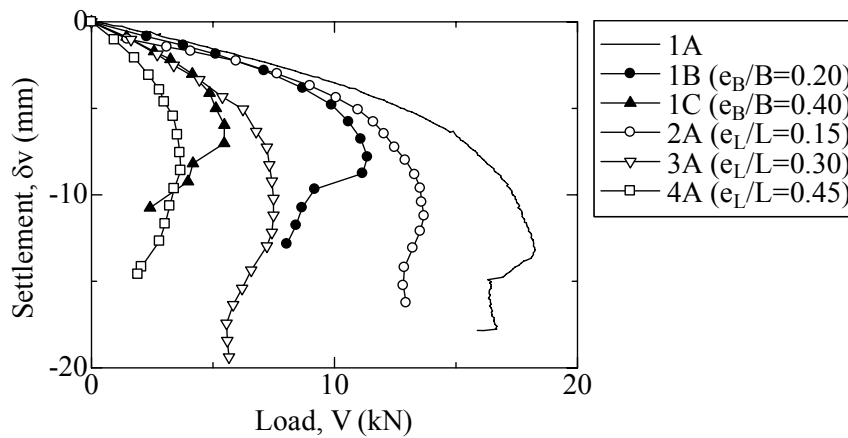
Figure 27. Load settlement curves for the single eccentricity cases (2A, 3A, 4A, 1B and 1C) with 1A.

Figure 28 is a similar plot but in terms of the ratio of failure load under eccentricity (Q_e) to that of without eccentricity (Q). The data of Terashi et al. (1984), Okamura et al. (2002) and the present study are presented in Figure 28. The solid line in Figure 28 is Meyerhof's hypothesis $q_e/q = (1-2e/B)^2$ for strip footing. Two observations can be made from the figure: one is Meyerhof's hypothesis is conservative, the other is that the data of rectangular footing with a smaller aspect ratio deviate more from the solid line presenting Meyerhof's hypothesis.

20
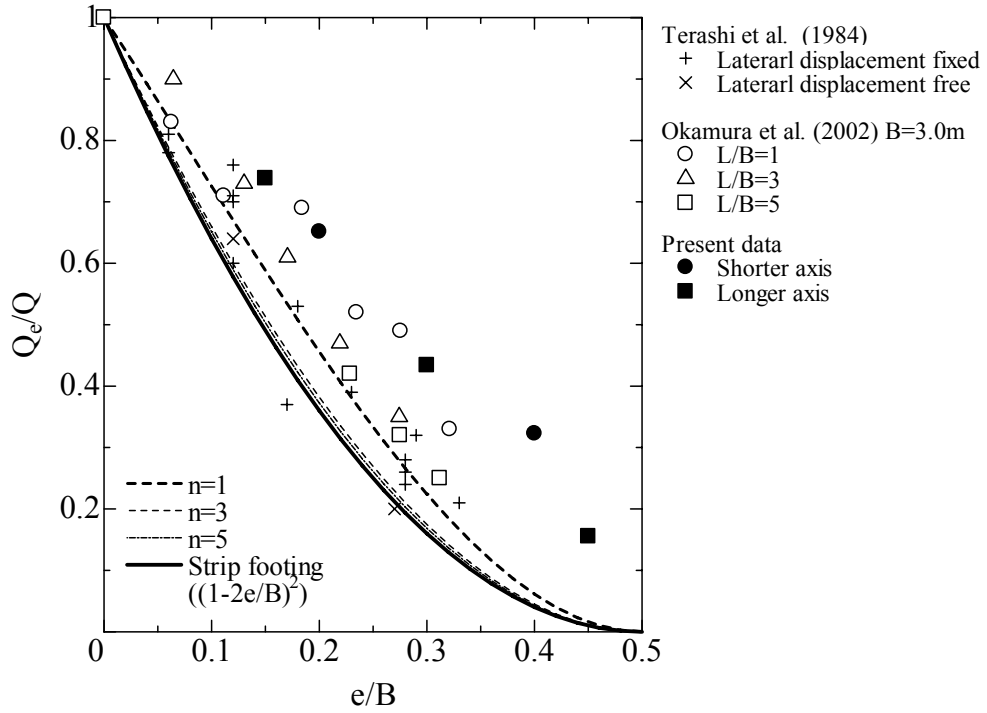
Figure 28. Relationships between eccentricity and failure load

For the cases of double eccentricity (Case 6 (2B), Case 7 (2C), Case 9 (3B), Case 10 (3C), Case 12 (4B) and Case 14 (4C)), the load-settlement curves are presented in Figure 29.
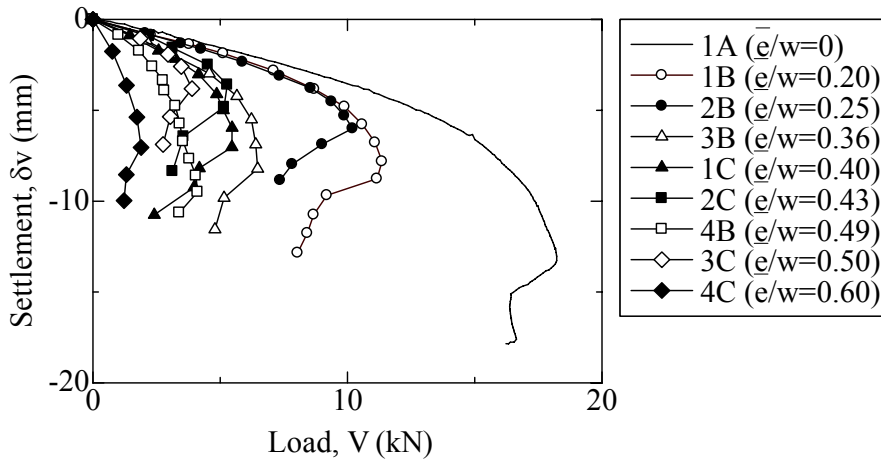
Figure 29. Load settlement curves for the double eccentricity cases (2B, 2C, 3B, 3C, 4B and 4C)

The settlements are normalized by the diagonal length of the footing w. From the figure, it is also said that the failure load and the vertical stiffness decrease with increasing the newly defined resultant eccentricity, $\overline{e}$, even for the double eccentricity. Figure 30 presents the decreasing trend of failure load with the increase of the resultant eccentricity. The regression curve for the line is found to be:

$$\frac{Q_e}{Q} = 1.00 - 2.12\left(\frac{\overline{e}}{w}\right) + 1.04\left(\frac{\overline{e}}{w}\right)^2.$$

(12)

21

For practical use, the equation (13) may be modified as:

$$\frac{Q_e}{Q} = \left(1 - \frac{\overline{e}}{w}\right)^2 . \tag{13}$$
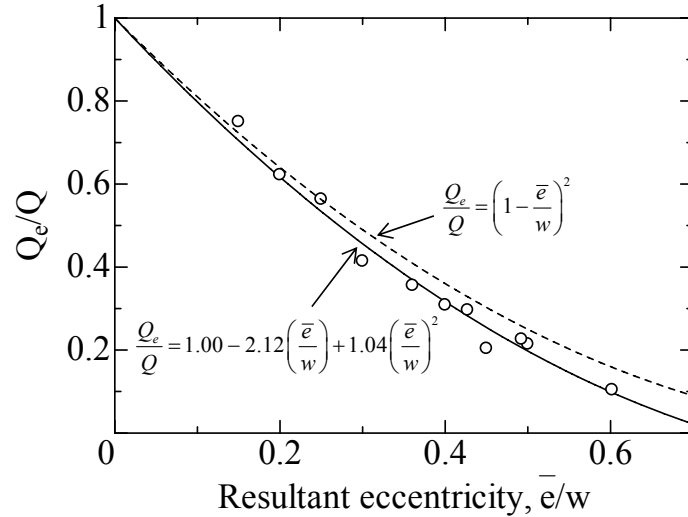
Figure 30. Relationship between failure load and the resultant eccentricity

Figure 31 shows the plan view of the extent of the zone of failure appeared at the ground surface determined by visual observation as well as the surface movement measured by the potentiometers for the cases of single eccentricity (Case 3(1B), Case 4(1C), Case 5(2A) and Case 11(4A)).
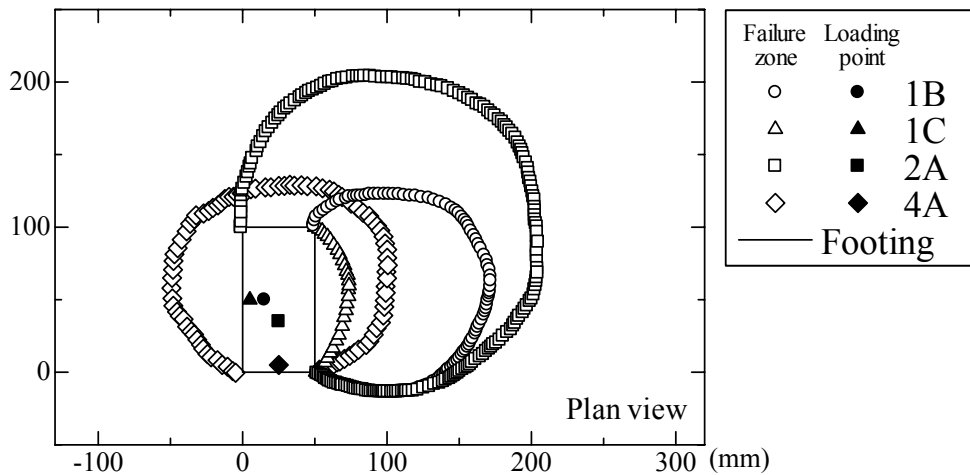
Figure 31. Zone of failure appeared at the ground surface for 1B, 1C, 2A and 4A

Generally, it is said that the area of failure zone decreases as the eccentricity increases, as was implied by the failure load. The failure zone starts from the right side corners of the footing for Case 3 (1B) and Case 4 (1C), whereas the failure zone develops from the bottom corners for Case 11 (4A). For these three cases, the predominant axis of the zone of failure almost coincides with the direction of eccentricity. In contrast, the failure zone for Case 5 (2A) exhibits more three dimensional mode; the failure zone develops from the upper left corner of the footing and ends at the lower right corner. Figure 32 presents the zone of failure for double eccentricity (Case 7(2C), Case 10(3C) and Case 13(4C)).
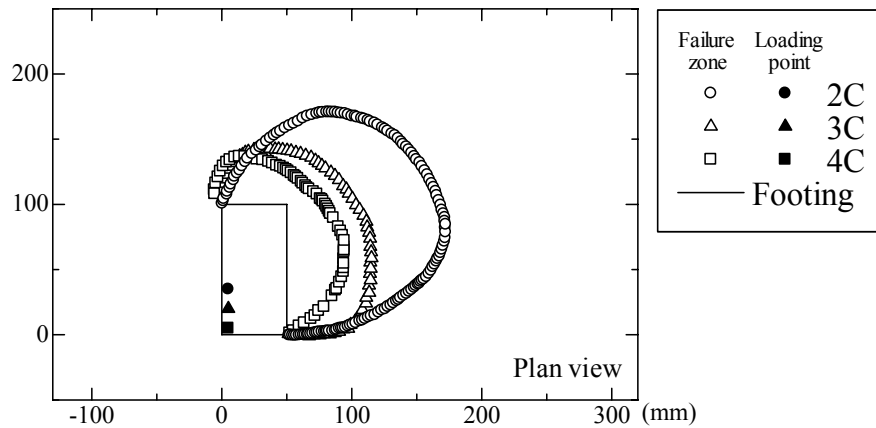
Figure 32. Zone of failure appeared at the ground surface for 2C, 3C and 4C

Once again it is confirmed that the zone of failure becomes smaller with increasing eccentricity. All their failure zones start at the two edges; one from the lower right corner of the footing and the other from the upper left corner. It suggests therefore that the diagonal length of the footing, w, may be an index of the extent of the failure zone at least for double eccentricity.

From a series of photographs, the coordinates of points of discontinuity clearly identified by the colored layer were read for various sections shown in Figure 24 and a program called AVS express 7.2 was use to compile the measured data and visualize the three dimensional failure mode for the cases of Case 16 (4A) for single eccentricity and Case 17 (4C) for double eccentricity, as are given in Figure 33 (a) and (b). Type B failure mode is clearly seen in Figure 33 (a) for single eccentricity. However the failure mode of rectangular footing is really in three dimensional in nature. The zone of heave shown in light grey is observed on the no eccentricity direction as well as on the opposite side of eccentricity. The failure mode for double eccentricity is more complicated as is seen in Figure 33 (b). The zone of heave first appears around the footing and then occurs slightly away from the footing as the footing further settles. This kind of progressive nature of the failure mechanism was reported earlier (Eastwood, 1955). The observed three dimensional failure mode experimentally observed presented here provides an opportunity for people to compare their numerical results, such as three dimensional FEM analysis of bearing capacity (Evans and Griffiths, 2005).
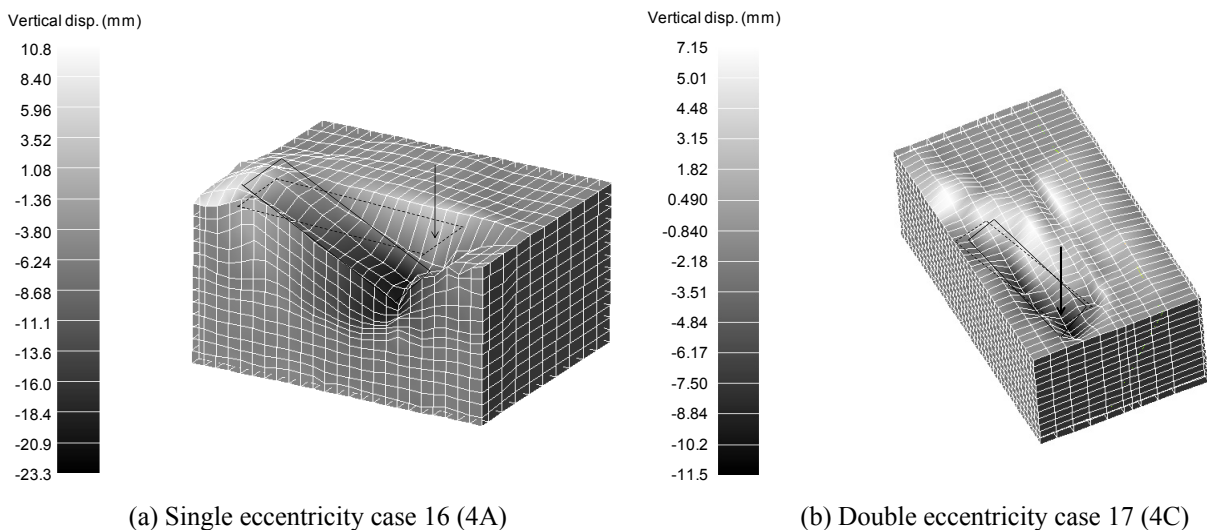
(a) Single eccentricity case 16 (4A)   (b) Double eccentricity case 17 (4C)

Figure 33. Three dimensional visualization of failure mode

4. Concluding remarks

   This paper presented recent studies of bearing capacity of shallow footing under combined loading conducted at the Tokyo Institute of Technology. The first FEM study is part of the graduation study by Mr.T.Takayanagi, while the second centrifuge study is part of the Master study by Mr. R. Bando. More detailed information is available in our recent papers (Takayanagi, et al.2009; Bando et al. 2010). The authors express their thanks to Dr. J. Izawa and Mr. S. Seki for their supports during the above studies.

References
1. Bando, R. Izawa, J and Kusakabe, O. (2010): Rectangular footing on sand subjected to double eccentric load, International Journal of Physical Modelling in Geotechnics (to appear).
2. Bolton, M. (1979): A guide to soil mechanics, London, MacMillan, pp. 323-324.
3. Bransby, M. F. and Randolph, M. F. (1998): Combined loading of skirted foundation, Geotechnique, 48(5), pp. 637-655.
4. Brown, J. D. and Meyerhof, G. G. (1969): 'Experimental study of bearing capacity in layered clays', Proc. of 7th International Conference on Soil Mechanics and Foundation Engineering, Vol.2, pp. 45-51.
5. Butterfield, R. and Gottardi, G. (1994): A complete three dimensional failure envelope for shallow footings on sand, Geotechnique 44, No. 1, pp.181-184.
6. Button, S. J. (1953): The bearing capacity of footings on a two-layered cohesive subsoil, Proc. of 3rd International Conference on Soil Mechanics and Foundation Engineering, Vol.1, pp. 332-335.
7. Chen, W. F. (1975): Limit analysis and soil plasticity, Elsevier, Amsterdam, The Netherlands.
8. Eastwood, W. (1955): The bearing capacity of eccentrically loaded foundations on sandy soils, Structural Engineer 23, No. 6, pp. 181-187.
9. Evans, M. D. and Griffith, D. V. (2005): 3D finite element analysis of bearing capacity failure in clay, Proceedings of 16th International Conference on Soil Mechanics and Geotechnical Engineering, Osaka, Vol. 2, pp. 893-896.
10. Georgiadis, M. and R. Butterfield. (1988): Displacements of footings on sand under eccentric and inclined loads, Canadian Geotechnical Journal 25, No. 2, pp. 199-212.
11. Japan Road Association. (2002): Specifications for Highway Bridges, Maruzen, pp. 276-279
12. Kim, J. K., Yang, T. S., Baek, W.J. and Lee, S. (2008): Estimating bearing capacity for dredged and reclaimed ground, Proc. of 6th Asian Young Geotechical Engineers Conference, pp. 240-250.
13. Kitazume, M. (1984): Influence of loading condition on bearing capacity and deformation, Proceedings of International Symposium on Geotechnical Centrifuge Model Testing, Tokyo, pp. 149-151.
14. Kitazume, M. and Ikeda, T. (1993): Influence of horizontal restriction in eccentric loading test, Domestic edition of Soils and Foundations 33, No.3, pp. 187-195. (in Japanese)
15. Merifield, R. S., Sloan, S. W. and Yu, H. S. (1999): Rigorous plasticity solutions for the bearing capacity of two layered clays, Geotechnique, 49, pp. 471-490.
16. Meyerhof, G. G. (1953): The bearing capacity of foundations under eccentric and inclined loads, Proceedings of 3rd International Conference on Soil Mechanics and Foundation Engineering, Switzerland, 1, pp. 440-445.
17. Michalowski, R. L. and Shi, L. (1995); Bearing capacity of footings over two-layer foundation soils, Journal of Geotechnical Engineering Division, ASCE, 121(5), pp. 421-427.
18. Musso, A. and Ferlisi, S. (2009): Collapse of a model strip footing on dense sand under vertical eccentric loading, Geotechnical and Geological Engineering 27, No. 2, pp. 265-279.
19. Nakase, A., Kimura, T., Saitoh, K., Takemura, J. and Hagiwara, T. (1987): Behaviour of soft clay with a surface crust, Proc. of   8th Asian Regional Conference on Soil Mechanics and Foundation Engineering, Vol. 1, pp. 401-404.
20. Narita, K and Yamanguchi, H. (1988): Analysis of bearing capacity for logarithmic spiral slip surfaces, Research Report of Aichi Institute of Technology, Vol. 23B, pp. 189-200. (in Japanese)
21. Nova, R. and Montransio, L. (1991): Settlement of shallow foundations on sand, Geotechnique 41, No. 1, pp. 243-256.
22. Okamura, M., Mihara, A., Takemura, J. and Kuwano, J. (2002): Effects of footing size and aspect ratio on the

bearing capacity of sand subjected to eccentric loading, Soils and Foundations 42, No.4, pp. 43-56.

23. Poulos, H. G., Carter, J. P. and Small, J. C. (2001): Foundations and retaining structures - Research and practice, Proceedings of 15th International Conference on Soil Mechanics and Foundation Engineering, Istanbul, 2001, 4. pp. 2527-2606.

24. Prakash, S. and Saran, S. (1971): Bearing capacity of eccentrically loaded footings, Journal of Soil Mechanics and Foundations Division ASCE 97, No. 1, pp. 95-117.

25. Purkayastha, R.D. and Char, A.N. (1977): Stability analysis for eccentrically loaded footings, Journal of Geotechnical Engineering Division ASCE 103, No. 6, pp. 647-651.

26. Reddy, A.S. and Srinivasan, R.J. (1967): Bearing capacity of footings on layered soils, Soil Mech. Found. Div, ASCE, 93(2), pp. 83-99.

27. Shiraro, M., Kouno, T., Asai, R., Nakatani, S., Fukui, J. and Paolucci, R. (2009): Large-scale Experiments on Nonlinear Behavior of Shallow Foundations Subjected to Strong Earthquakes, Soils and Foundations 48, No. 5, pp. 673-692.

28. Taiebat H. and Carter J.P. (2000): Numerical studies of the bearing capacity of shallow footings on cohesive soil subjected to combined loading, Geotechnique, 50 (4), pp. 409-418.

29. Takayanagi, T., Izawa, J. and Kusakabe, O. (2009): Bearing capacity of strip footing on clay layered ground under combined loading, Indian Geotechnical Journal 39, No. 4, pp. 341-359.

30. Tan, F.S. (1990): Centrifuge and theoretical modeling of conical footing on sand, Ph. D thesis, Cambridge University.

31. Terashi, M., Kitazume, M and Tanaka, H. (1984): Applications of PHRI Geotechnical Centrifuge, Proceedings of International Symposium on Geotechnical Centrifuge Model Testing, Tokyo, pp. 164-171.

32. Wang, C. X., and Carter, J. P. (2002): Deep penetration of strip and circular footings into layered clays. International Journal of Geomechanics, 2(2), pp. 205-232.

33. Zhu, M. and Michalowski, R.L.(2005): Shape factors for limit loads on square and rectangular footings. Journal of Geotechnical and Geoenvironmental Engineering, ASCE, 131(2), pp. 223-231.